SCIENTIFIC REPORTS

OPEN

SUBJECT AREAS:
MINERALOGY
SOLID-STATE CHEMISTRY

Received
31 July 2013

Accepted
13 September 2013

Published
2 October 2013

Correspondence and requests for materials should be addressed to N.I. (ishizawa@nitech.ac.jp)

Structural evolution of calcite at high temperatures: Phase V unveiled

Nobuo Ishizawa[1], Hayato Setoguchi[1] & Kazumichi Yanagisawa[2]

[1]Advanced Ceramics Research Center, Nagoya Institute of Technology, 10-6-29 Asahigaoka, Tajimi, 507-0071, Japan, [2]Research Laboratory of Hydrothermal Chemistry, Kochi University, 2-17-47 Asakurahoncho, Kochi, 780-8073, Japan.

The calcite form of calcium carbonate $CaCO_3$ undergoes a reversible phase transition between $R\bar{3}c$ and $R\bar{3}m$ at ~1240 K under a CO_2 atmosphere of ~0.4 MPa. The joint probability density function obtained from the single-crystal X-ray diffraction data revealed that the oxygen triangles of the CO_3 group in the high temperature form (Phase V) do not sit still at specified positions in the space group $R\bar{3}m$, but migrate along the undulated circular orbital about carbon. The present study also shows how the room temperature form (Phase I) develops into Phase V through an intermediate form (Phase IV) in the temperature range between ~985 K and ~1240 K.

Preceding Bragg's deduction in 1914 about the room-temperature atomic configuration of the calcite form of calcium carbonate $CaCO_3$ (Phase I)[1], Boeke found in 1912 a reversible phase transition at around 1243 K[2]. Since then, many experiments have been undertaken to determine the high-temperature structure of calcite and have indeed come very close to the final goal[3], but none have succeeded in determining its true structure, for the following reason. In addition to the experimental difficulties associated with the instability of calcite tending towards decomposition into calcium oxide and carbon dioxide even under a CO_2 atmosphere up to ~0.4 MPa, the oxygen atoms do not sit at rest at the specific atom positions defined by the space group. Here we show the structure of the high temperature modification of calcite, named as Phase V by Mirwald[4], in addition to the intermediate state (Phase IV) bridging Phases I and V. This study contributes, not only to crystallographic science, but also to a wider area including the carbon cycle of the earth, as the carbonate materials, being the abundant solid state container of carbon dioxide gas, are expected to follow a similar route of decarbonation as seen with calcite, irrelevant to temperature or atmosphere.

Results

The *in-situ* single-crystal X-ray diffraction experiments were carried out on calcite crystals at various temperatures up to ~1300 K under a CO_2 or air atmosphere (Tables S1–S4). The *hk*0 and *hk*1 reciprocal sections in the hexagonal setting at selected temperatures (Fig. 1) showed, in addition to the Bragg spots ascribed to the $R\bar{3}c$ symmetry, diffuse scattering around reciprocal points with non-integer indices, which correspond to the 'F points' of the Brillouin zone of the $R\bar{3}m$ parent lattice[5]. These diffuse F peaks became prominent upon heating. On the other hand, the *hkl* reflections with l = odd ('Z points' of the $R\bar{3}m$ parent lattice) gradually weakened upon heating as first reported by Tsuboi[6] in 1927. The Z points barely existed at 1234 K and completely disappeared in the image taken at 1275 K (Fig. 1). This extinction provides the $R\bar{3}m$ symmetry for the crystal in Phase V. On the other hand, the diffuse F peaks still remained after the completion of transition into Phase V, as evidenced in the same 1275 K image. This suggests that they do not originate from the $R\bar{3}c$–$R\bar{3}m$ transition but underlie all the calcite variants. The transition temperature was estimated to be 1240 K from the linear extrapolation of the fourth power of the observed structure factor of the 113 reflection against temperature (Fig. S1**c**). Crystals in Phase V survived in a limited temperature range of ~35 K between 1240–1275 K, while precipitating a small amount of CaO powder under a CO_2 atmosphere of ~0.4 MPa (Fig. S2**a**). The Phase I–IV–V transitions seemed reversible because the crystal cooled from 1275 K completely recovered the Phase I structure. Further heating above 1275 K, on the other hand, caused the crystals a rapid decomposition into the CaO solid and CO_2 gas without changing their apparent parallelepiped morphology (Fig. S2). Temperature dependencies of the cell dimensions were similar to those reported previously in detail[7,8] (Fig. S1**a**–**b**).

The structure of Phase I consists of Ca1 at (0, 0, 0), C1 at (0, 0, 1/4) and O1 at (x, 0, 1/4) with x ~ 0.25 in the space group $R\bar{3}c$[1,9–11] (Fig. 2**a**). All the carbonate groups on a plane parallel to (001) have the same orientation, whereas those in the adjacent planes have the inverse orientation with respect to the one in between. These

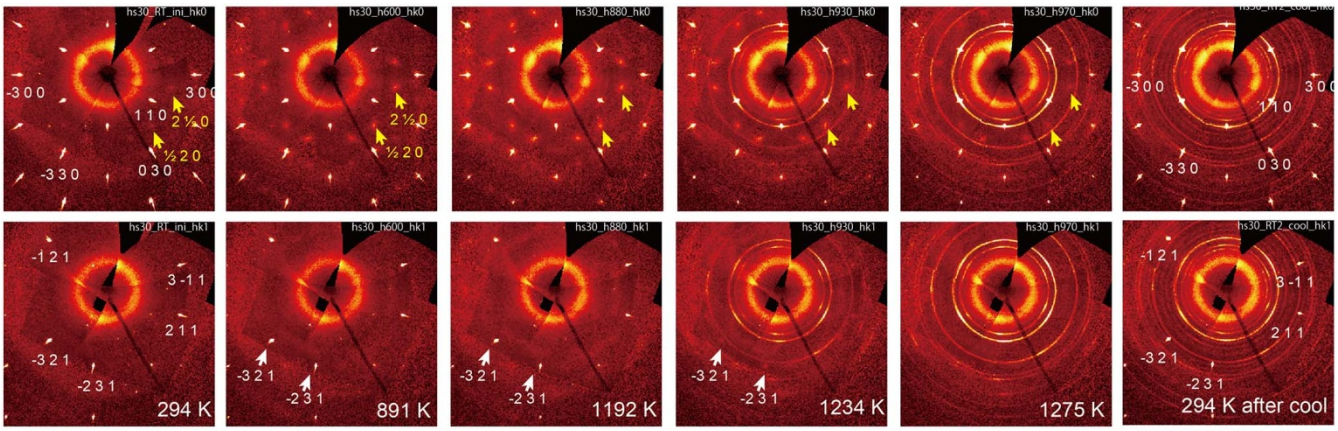

Figure 1 | Selected reciprocal sections of calcite upon heating and cooling. The *hk*0 (top) and *hk*1 (bottom) reciprocal sections of calcite (hs30) in the hexagonal setting, reconstructed from the two dimensional flame data at temperatures of 294 and 891 K (Phase I), 1192 and 1234 K (Phase IV) and 1275 K (Phase V) attained upon heating, and 294 K (Phase I) after cooling. Several Bragg spots are indexed based on the R$\bar{3}$c unit cell. Several diffuse 'F' points are also indexed, for example, 2 1/2 0, with yellow arrows.

different orientations are illustrated using different colours (blue and lime) for the O1 atoms. The structure of Phase IV also belongs to R$\bar{3}$c but contains two different O atom sites in a disordered way at the Wyckoff notation 18*e*: O1 (x, 0, 1/4) and O2($-x$, 0, 1/4) with $x \sim 0.25$. In Fig. 2**b**, two different orientations of the CO_3 groups are shown with the O atoms in blue and lime, in accordance with the colour scheme used in Fig. 2**a**. It should be noted that the two kinds of carbonate molecules in disorder are not in the 60° or 180° rotation relationships as often mentioned in literature, but in the improper relationship; the two molecules are geometrically related by the inversion at carbon, as evidenced by their atomic displacement parameter (ADP) ellipsoids (Fig. 2**b** and Fig. S3**a**).

The joint-probability density function was calculated from the inverse Fourier transform of the anharmonic ADPs approximated by the 3rd order expansion of the Gram–Charlier series[12]. The effective one particle potential was then obtained from the probability density function using Boltzmann statistics[13]. The potential profiles of the O triangle of the CO_3 group (Fig. 3**a**–**b**) show thee deep minima at the O1 sites in Phase I, with a slight elongation along the O circle about carbon. On the other hand, the ridges separating the O1 sites become supressed upon heating in Phase IV, allowing existence of a small portion of O atoms at O2 sites. The potential barrier along the O circle changes with temperature (Fig. 3**c**), from which we could evaluate the activation energy as a function of temperature when the O atom hops between the O1 and O1′ sites. The activation energy of approximately 1 eV in Phase I is high enough to disable the migration of O atoms along the O circle. The single sharp ridge in Phase I becomes dented in Phase IV and splits into two gentle ridges between the O1 sites. These potential barriers become lower and shift towards the midpoint between O1 and O2 upon heating. The activation energy as a function of temperature (Fig. 3**d**) indicated a large drop of ~0.5 eV between 974 K and 995 K, from which the I–IV phase transition temperature was deduced to be ~985 K. The population of O atoms at O2 sites increased upon heating, with decreasing activation energy (Fig. 3**d**). The highest temperature of 1073 K that Markgraf and Reeder[11] investigated is still at the

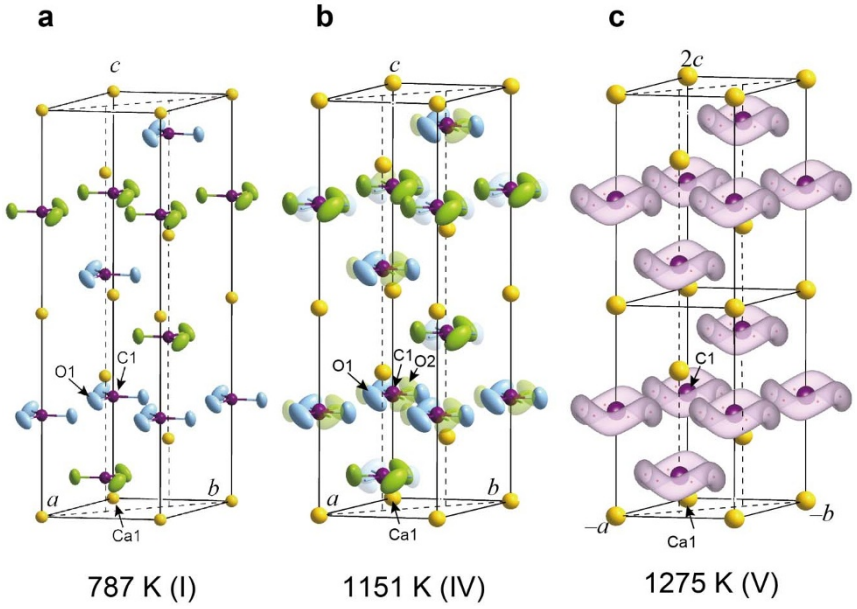

Figure 2 | Structures of calcite. (a), Phase I at 787 K, (b), Phase IV at 1151 K, (c), Phase V at 1275 K. The ADP ellipsoids are drawn at the 50% probability level. The O atoms in Phase V are represented by the 50% probability isosurface of the joint probability density function. Two unit cells along (c) are drawn for Phase V in the orientation, $a_V = -a_I$ and $b_V = -b_I$, so that Phase V has an atom arrangement similar to those of Phases I and IV. This makes up for the change in the obverse–reverse relationships caused by the halving of the R$\bar{3}$c unit cell along c.

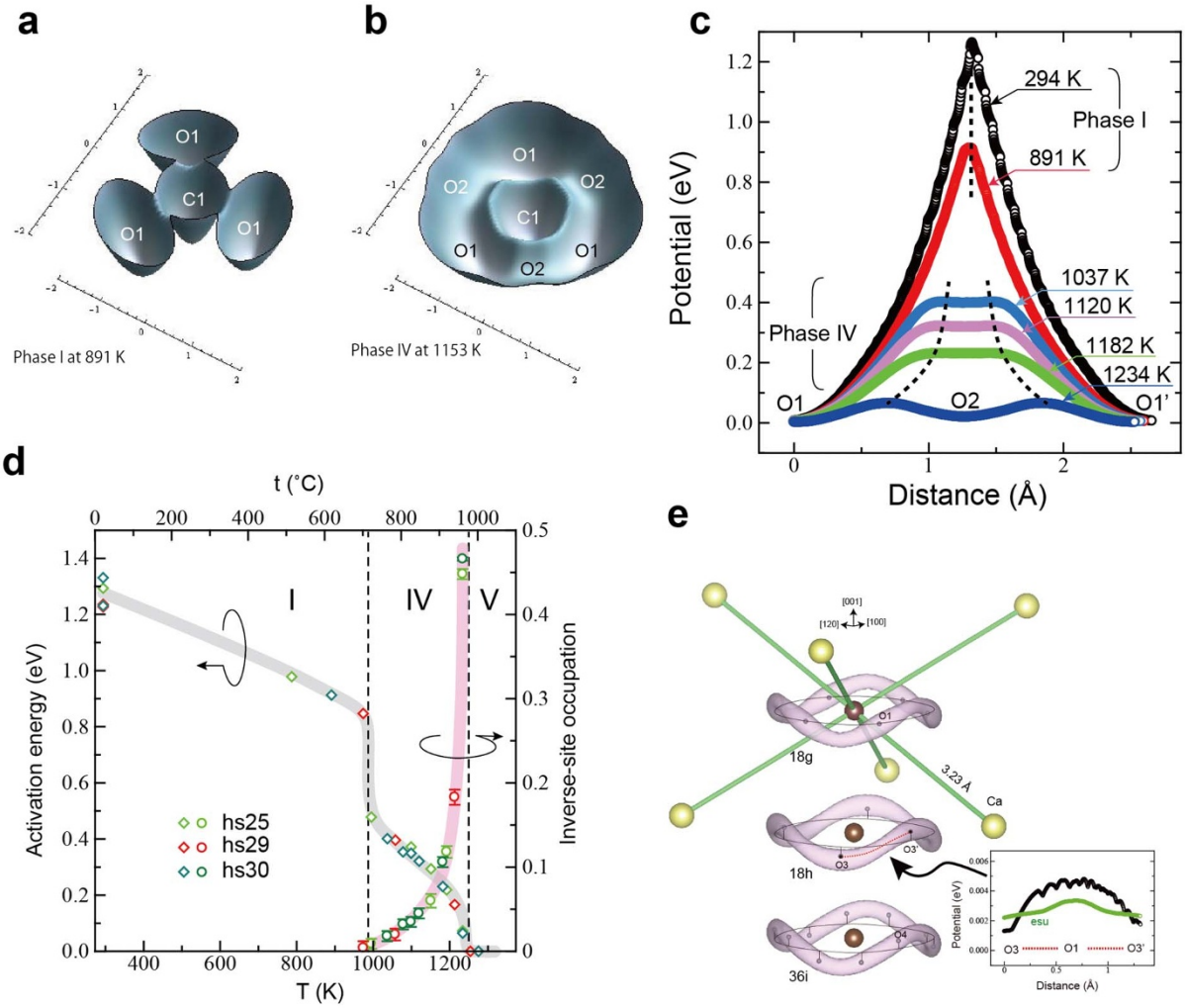

Figure 3 | Potentials and the activation energy. (a), Potential surface of the 4 Å × 4 Å square section (carbon at its centre) for Phase I at 891 K (hs30). (b), That for Phase IV at 1153 K (hs30). The depth profiles in (a) and (b) are plotted in the range 0–0.7 eV. (c), Potential curves at selected temperatures (hs30) along the arc O1–O2–O1 in (b). Dashed lines indicate the expected traces of potential maxima in Phases I and IV. (d), The activation energy (eV) of the O atom along the O circle about carbon and the population of the inverse site (O2) in Phase IV as a function of temperature. (e), The 10% isosurface of the joint probability density function of O atoms about carbon in the models 18g, 18h and 36i for Phase V at 1275 K (hs30). The six Ca atoms surrounding the CO_3 group at 3.23 Å are also drawn in the model 18g. The inset shows changes in potential energy (eV) along the dashed line in the undulated circular orbital with estimated standard uncertainties in green colour.

incipient period of Phase IV, where the O2 population is only ~1%. This is in agreement with a recent powder diffraction study[8]. Attainment of equal populations of O1 and O2 at the high temperature side of Phase IV means that the two moieties, $0 \leq z \leq 1/2$ and $1/2 \leq z \leq 1$ of the $R\bar{3}c$ unit cell become identical, resulting in a halved cell with the $R\bar{3}m$ symmetry. This does not mean, however, that Phase V is a completely disordered version of Phase IV.

The difference Fourier synthesis with phases calculated from the Ca and C positions revealed residual electron densities distributed along an undulated circular orbital about carbon (Fig. S4**b**). This undulated orbital was modelled into three different arrangements of the O atoms in association with the use of anharmonic ADPs, as shown in Fig. 3**e**: 1) Model 18g assuming half occupied O1 at Wyckoff position 18*g* (x, 0, 1/2) of the space group $R\bar{3}m$, 2) Model 18h assuming half occupied O3 at 18*h* (x, $-x$, z), 3) Model 36i assuming quarterly occupied O4 at the general position 36*i* (x, y, z).

All these models gave similar reliability factors in the refinements. Moreover, they gave approximately the same joint probability density function regardless of the difference in the O atom positions. This indicates that the O atom does not sit still at a position specified by each model, but it can be located anywhere along the undulated circular orbital about carbon with equal probability. This 'itinerant' feature was also confirmed by the potential calculation along the undulated orbital (Fig. 3**e** inset). We saw in Phase IV that the O atom could migrate along the O circle by the hopping mechanism given the energy surpassing 0.2–0.4 eV. On the other hand, the potential curve in Phase V neither exceeds ~0.005 eV at any point, nor does it form a significant barrier exceeding three times of the estimated uncertainties. This means that the O atom can freely migrate along the undulated orbital about carbon without any energy for activation.

Discussion

The undulation of the O orbital presumably occurs in order to minimise the repulsion between the Ca and O electron clouds. As shown in Fig. 3**e**, the O orbital undulates as if avoiding the lines connecting Ca and C. The shortest Ca–O distances are 2.45, 2.38 and 2.37 Å for the models 18g, 18h and 36i, respectively. If no undulation is assumed, i.e., $z = 1/2$ for O in the models 18h and 36i, the shortest Ca–O distances become 2.27 and 2.26 Å, respectively, being ~5% shorter than the undulated models and even shorter than the Ca–O distance of 2.36 Å in calcite at room temperature. Therefore, the undulation seemingly succeeds in realising reasonably long Ca–O

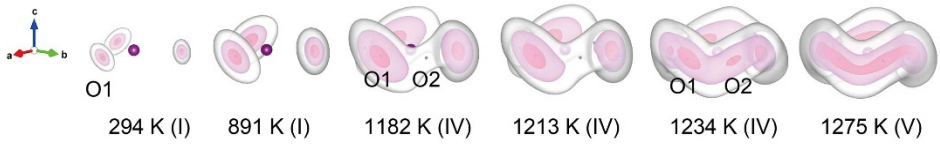

Figure 4 | The isosurface plots of the joint probability density function of O atoms around carbon. Data plotted are at 294 and 891 K for Phase I, 1182, 1213, and 1234 K for Phase IV, and 1275 K for phase V. All data are calculated from the hs30 datasets, except for those at 1213 K from hs29. The isosurface levels are top 10% (red), 50% (pink) and 90% (white) probabilities from inside. The crystallographic (a) and (b) directions of the axes label are reversed in Phase V as explained in the caption of Fig. 2.

distances at any point of the orbital compared with the flat one. The undulation of the orbital along the c axis at 1275 K is ±0.18(1) Å at the maximum, which makes the inclination angles of ±7.7(1)° for the C–O bond with respect to the basal plane. This sort of umbrella inversion between +7.7° and −7.7° (Fig. S3**b**) associated with the assumed rotational migration would drive the crystal to decarbonation shortly.

Finally, we stress the importance of the joint probability density function rather than the conventional ball-and-stick model in order to distinguish the Phases I, IV and V (Fig. 4). The three O1 atoms around carbon exist in an isolated manner in Phase I. The tail of the joint probability density function gradually extends to cover the O2 site in Phase IV. Although a portion of the O atoms can actually occupy the O2 site orienting to the inverse direction against the O1 triangle in Phase IV, the O1 and O2 atoms are still vibrating about their mean positions on the plane where carbon lies. Upon further heating, the joint probability density function is completely connected to form the undulated orbital in Phase V. The O atom sublattice is premelted and the positions become unable to be allocated specifically to any Wyckoff sites with fixed coordinates. The O atoms exist just as a probability along the undulated orbital about carbon. The present study has thus unveiled the Phase V structure of calcite, which stands as a crystal at the very last minute before decomposition.

Methods

Crystal growth. Reagent grade $CaCO_3$ powder (5.00 g) was placed in a 1.4 L Teflon-lined stainless steel autoclave with 1050 mL of 5 M NH_4NO_3 at pH 7.5. The autoclave was heated to 418 K for 7 h with agitation of a rotator at 250 rpm to dissolve the calcite powder completely, followed by cooling at a rate of 2.5 K/h to room temperature. The products were then washed with deionised distilled water and filtered using a 150 μm sieve. Spectroscopic analysis using a JED-2300 instrument (Jeol Ltd.) revealed no significant impurities in the calcite crystals.

Diffraction experiments. Single-crystal X-ray diffraction experiments were carried out on several calcite crystals with a parallelepiped shape of ~200 μm edge length on average using an APEX II diffractometer (Bruker AXS Inc.) equipped with a charge-coupled device X-ray detector and a high temperature apparatus[14]. Shield tube Mo Kα was used with the 0.3 φ monocap capillary collimator. The hs11 datasets were collected in an open air atmosphere up to 787 K using a crystal mounted on a silica glass capillary with the adhesive cement. The hs25, 29 and 30 datasets were collected using crystals which were each encapsulated in a thin 0.2–0.3 φ silica glass capillary under the CO_2 atmosphere. No adhesive was necessary in this case because the crystal was always kept in tight contact with the inner wall of capillary at elevated temperatures and rarely slipped, owing to the difference in thermal expansion between the crystal and the silica glass (Fig. S2**a**). The CO_2 pressure in the sealed capillary was estimated to be ~0.4 MPa at ~1300 K from the pressure–temperature law for the ideal gas. The crystal in capillary was placed in a hot air stream, the temperature of which was monitored by the Pt/Pt13%Rh thermocouple. The sample temperature was calibrated using the 3rd order polynomial according to our previous study[15]. The accuracy of the transition temperature 1240 K was estimated to be approximately ±5 K. A set of frame data at a constant temperature was collected for 3–5 h up to $2\theta < 60°$ for the hs11 and hs25 datasets, $2\theta < 80°$ for hs29 and $2\theta < 70°$ for hs30.

Data analysis. Crystallographic calculations were primarily conducted using Jana2006[16]. Vesta[17], Diamond (Crystal Impact GbR) and Mathematica (Wolfram Research, Inc) were used for graphical representations and other subsidiary calculations. Extinction corrections were applied on the basis of the Becker & Coppens[18] formalism (Type I) to the Phase I datasets. The extinction effect was negligibly small for the Phase IV and V datasets. In parallel with the anharmonic ADP refinements, the translation-libration-screw (TLS) refinements[12], using a symmetric 3 × 3 translation tensor **T**, the symmetric 3 × 3 libration tensor **L** and the nonsymmetric 3 × 3 screw tensor **S**, were carried out assuming a rigid body model for the CO_3 group with the 321 point symmetry. Further details are given in Supplementary information.

1. Bragg, W. L. The analysis of crystals by the X-ray spectrometer. *Proceedings of the Royal Society of London. Series A* **89**, 468–489 (1914).
2. Boeke, H. E. Die Schmelzerscheinungen und die umkehrbare Umwandlung des Calciumcarbonats. *Neues Jahrb. Mineral.* **1**, 91–121 (1912).
3. Dove, M. T., Swainson, I. P., Powell, B. M. & Tennant, D. C. Neutron powder diffraction study of the orientational order–disorder phase transition in calcite, $CaCO_3$. *Phys. Chem. Minerals* **32**, 493–503 (2005).
4. Mirwald, P. W. A differential thermal analysis study of the high-temperature polymorphism of calcite at high pressure. *Contr. Mineral. and Petrol.* **59**, 33–40 (1976).
5. Hagen, M., Dove, M. T., Harris, M. J., Steigenberger, U. & Powell, B. M. Orientational order-disorder phase transition in calcite. *Physica B: Condensed Matter* **180–181**, 276–278 (1992).
6. Tsuboi, C. On the Effect of temperature upon the crystal Structure of calcite. *Proceedings of the Imperial Academy (Japan)* **3**, 17–18 (1927).
7. Dove, M. T. & Powell, B. M. Neutron diffraction study of the tricritical orientational order/disorder phase transition in calcite at 1260 K. *Phys. Chem. Minerals* **16**, 503–507 (1989).
8. Antao, S. M., Hassan, I., Mulder, W. H., Lee, P. L. & Toby, B. H. In situ study of the R-3c to R-3m orientational disorder in calcite. *Phys. Chem. Minerals* **36**, 159–169 (2009).
9. Wyckoff, R. W. G. The crystal structures of some carbonates of the calcite group. *American Journal of Science, Series 4* **50**, 317–360 (1920).
10. Maslen, E. N., Streltsov, V. A. & Streltsova, N. R. X-ray study of the electron density in calcite, $CaCO_3$. *Acta Crystallogr., Sect. B: Struct. Sci.* **49**, 636–641 (1993).
11. Markgraf, S. A. & Reeder, R. J. High-temperature structure refinements of calcite and magnesite. *Amer. Mineral.* **70**, 590–600 (1985).
12. Willis, B. T. M. & Pryor, A. W. *Thermal vibrations in crystallography.* (Cambridge University Press, 1975).
13. Zucker, U. H. & Schulz, H. Statistical approaches for the treatment of anharmonic motion in crystals. I. A comparison of the most frequently used formalisms of anharmonic thermal vibrations. *Acta Crystallogr., Sect. A: Found. Crystallogr.* **38**, 563–568 (1982).
14. Ishizawa, N. *et al.* Development of high-temperature single-crystal X-ray diffraction system for electron density distribution analyses. *Annu. Rep. CRL 2006, Nagoya Inst. Technol.* **6**, 12–18 (2007).
15. Wang, J. W., Hibino, H. & Ishizawa, N. Temperature calibration of the high-temperature single-crystal X-ray dffractometer. *Annu. Rep. CRL 2010, Nagoya Inst. Technol.* **10**, 43–47 (2011).
16. Petricek, V., Dusek, M. & Palatinus, L. *Jana2006, Structure Determination Software Programs* (Institute of Physics, Praha, Czech Republic, 2006).
17. Momma, K. & Izumi, F. VESTA 3 for three-dimensional visualization of crystal, volumetric and morphology data. *J. Appl. Crystallogr.* **44**, 1272–1276 (2011).
18. Becker, P. J. & Coppens, P. Extinction within the limit of validity of the Darwin transfer equations. I. General formalism for primary and secondary extinction and their applications to spherical crystals. *Acta Crystallogr., Sect. A: Found. Crystallogr.* **30**, 129–147 (1974).

Acknowledgements

We thank Dr Vaclav Petricek at the Institute of Physics, Academy of Science, Czech Republic, for his invaluable support with our data calculation and implementation of the Jana2006 program package, Ms. Tomomi Gotoda at Research Laboratory of Hydrothermal Chemistry, Kochi University, for her help with the growth of calcite crystals, Mr. Hisashi Hibino at Nagoya Institute of Technology, for his help with the EDS and SEM analyses, Associate Professor Jung Wang from the Inner Mongolia University of Technology, and Dr Terutoshi Sakakura from the Institute of Multidisciplinary Research for Advanced Materials, Tohoku University, Japan, for their help in the preliminary stage of this work. This work was supported by JSPS KAKENHI Grant number 22360272.

Author contributions

K.Y. conducted the hydrothermal growth of calcite crystals. H.S. conducted all the diffraction experiments at high temperatures and EDS/SEM experiments. N.I. carried out the remaining parts of the study.

Additional information

Supplementary information accompanies this paper at http://www.nature.com/scientificreports

Competing financial interests: The authors declare no competing financial interests.

How to cite this article: Ishizawa, N., Setoguchi, H. & Yanagisawa, K. Structural evolution of calcite at high temperatures: Phase V unveiled. *Sci. Rep.* **3**, 2832; DOI:10.1038/srep02832 (2013).

This work is licensed under a Creative Commons Attribution-NonCommercial-ShareAlike 3.0 Unported license. To view a copy of this license, visit http://creativecommons.org/licenses/by-nc-sa/3.0